

Exploring Dual-Sniffer Passive Localization: Algorithm Design and Experimental Results

Tuo Wu, Lingyu Hou, Hong Niu, Saihua Xu,
Sirajudeen Gulam Razul, Chau Yuen, *Fellow, IEEE*

Abstract—In this paper, we explore a dual-sniffer passive localization system that detects the timing difference of signals from both commercial base station (eNb) and user equipment (UE) to the sniffers. We design two localization schemes for UE localization: a time of arrival (ToA) based scheme and a time difference of arrival (TDoA) based scheme. In the ToA-based scheme, we derive two ellipse equations from measured arrival times at two sniffers, enabling direct numerical computation of the estimated position. For the TDoA-based scheme, we relocate one sniffer to a different position to obtain two sets of TDoA measurements, resulting in hyperbola equations. We then apply a least squares (LS) algorithm to analytically estimate the UE's position. Simulation results validate the effectiveness of the proposed TDoA-based scheme, demonstrating improved accuracy in UE positioning. We build a platform based on the considered localization system and conduct real-world experiments. The experimental results confirm the accuracy and practicality of the TDoA-based dual-sniffer localization scheme, demonstrating improved precision in passive localization.

Index Terms—Dual-sniffer, passive localization, ToA, TDoA.

I. INTRODUCTION

In the era of fifth-generation (5G) technology, there is an escalating need to accurately locate mobile devices such as smartphones within densely populated urban environments. Applications like navigation [1], security [2], and resource allocation [3] all rely on precise user equipment (UE) localization [4].

Software-defined radio (SDR) sniffers have emerged as vital tools for UE localization in both long-term evolution (LTE) and 5G networks. software-defined radio (SDR) sniffers have emerged as a vital tool for UE localization. Despite the rollout of 5G, LTE networks continue to be widely deployed and integrated within the existing infrastructure, making LTE sniffers still highly relevant for localization tasks in contemporary networks. However, existing open-source LTE sniffers, such as LTEye [5] and FALCON [6], primarily focus on decoding the downlink control channel and are incapable of capturing IP packets or critical cellular protocol packets like radio resource control (RRC) and non-access stratum (NAS). This limitation significantly reduces their applicability in scenarios that require full packet access, particularly in internet of things

(IoT) networks where comprehensive monitoring and analysis are crucial [7].

Fortunately, Kotuliak et al. in [8] introduced LTE Sniffer, an open-source tool suitable for UE localization in conjunction with commercial base stations (eNbs). Their approach involves mobile fingerprinting by extracting the international mobile subscriber identity (IMSI) of the UE using a dedicated database and a machine learning-based [9] IMSI extractor. However, this method necessitates building a database and consumes substantial resources. In applications such as security, where immediate localization of mobile devices via eNbs is essential, relying on extensive databases and resource-intensive processes poses a non-trivial challenge.

To address this challenge, we introduce a dual-sniffer system that detects the timing difference of signals from both the commercial eNb and the UE to the sniffers. By formulating a localization problem based on these time differences, we can accurately detect and locate the UE without the need for extensive databases or resource-intensive computations. The main contributions can be summarized as follows:

- We investigate a dual-sniffer localization system that detects the timing difference of signals from both the commercial eNb and the UE to the sniffers.
- We design two localization schemes for UE positioning: a time of arrival (ToA) based scheme and a time difference of arrival (TDoA) based scheme. In the ToA-based scheme, we derive two ellipse equations from the measured arrival times at the two sniffers, enabling direct numerical computation of the estimated position.
- For the TDoA based scheme, we relocate one sniffer to a different position to obtain two sets of TDoA measurements, resulting in two hyperbola equations. We then apply a least square (LS) algorithm to analytically estimate the position.
- We build the platform based on the considered localization system and conduct real experiments, which validates the effectiveness of the proposed TDoA based dual-sniffer localization scheme, demonstrating improved accuracy in passive localization.

II. SYSTEM MODEL

In a dual-sniffer localization system, the primary components include the UE, an eNb, and 2 sniffers (SNs). The eNb, serving as the main connection point for the UE within the LTE network, is located at a fixed and known position denoted by $\mathbf{p} = [x_p, y_p]^T$. The true location of the UE is represented by $\mathbf{u} = [x_u, y_u]^T$, which is unknown and requires estimation.

(Corresponding author: Chau Yuen.)

T. Wu, L. Hou, H. Niu, S. Xu and C. Yuen are with the School of Electrical and Electronic Engineering, Nanyang Technological University, 639798, Singapore (E-mail: {tuo.wu, e230033, hong.niu, SHXU, chau.yuen}@ntu.edu.sg).

S. G. Razul is with the Temasek Laboratories, Nanyang Technological University, Singapore 637553 (E-mail: esirajudeen@ntu.edu.sg).

It is assumed that the distance between the UE and the eNb is d_{UB} . Each sniffer, indexed by k where $k \in \{1, 2\}$, is strategically placed at a location $\mathbf{s}_k = [x_k, y_k]^T$. The distances from the k -th sniffer to the eNb and to the UE are denoted by $d_{eNb,k}$ and $d_{UE,k}$, respectively. These distances are calculated using the Euclidean distance formula as

$$d_{eNb,k} = \|\mathbf{s}_k - \mathbf{p}\| = \sqrt{(x_k - x_p)^2 + (y_k - y_p)^2}, \quad (1)$$

$$d_{UE,k} = \|\mathbf{s}_k - \mathbf{u}\| = \sqrt{(x_k - x_u)^2 + (y_k - y_u)^2}, \quad (2)$$

$$d_{UB} = \|\mathbf{u} - \mathbf{p}\| = \sqrt{(x_u - x_p)^2 + (y_u - y_p)^2}. \quad (3)$$

The sniffers are equipped to capture LTE signals transmitted between the eNb and the UE. The UE's location is estimated based on the propagation time of these signals and the TA command¹.

A. Transmission from eNb to UE

In the downlink transmission from the eNb to the UE, the eNb serves as the reference clock for synchronization. Specifically, the eNb transmits radio frames every 10 ms and subframes every 1 ms with negligible drift². Although the UE may have a lower-quality or less accurate internal clock, it synchronizes to the eNb's clock to ensure accurate reception of the time-sensitive downlink signals.

Let the transmission times from the eNb be defined as T_{BS} , representing the subframe timings, which can be formulated as

$$T_{BS} = \{t_0, t_1, \dots, t_n\}, \quad (4)$$

where n ($n \in \{1, 2, \dots, N\}$) is an integer representing the subframe index, and N denotes the total number of transmitted subframes.

Assuming the UE has already received the TA command from the eNb, it transmits uplink frames earlier than it receives the downlink frames to compensate for propagation delays. Specifically, if the eNb transmits a downlink frame at time $T_{BS} = t_n$, the UE transmits the corresponding uplink frame at

$$T_{UE} = t_n + \frac{d_{UB}}{c} - \delta_{TA} + \varepsilon_{UE}, \quad (5)$$

where c denotes the speed of light, δ_{TA} is the timing advance value provided by the eNb, and ε_{UE} represents any hardware timing error in the UE. It is important to note that δ_{UE} is not a timing offset because it is independent of the eNb's clock.

B. Transmission from eNb/UE to SNs

Next, we model the transmissions between the eNb and SNs, and between the UE and SNs. Notably, the SNs are not required to be synchronized with GPS for practical localization purposes.

¹The TA command, issued by the eNb, compensates for the signal propagation delay between the UE and the eNb by adjusting the timing of the uplink signals from the UE, ensuring synchronization with the eNb's receiving window.

²The eNb employs a free-running clock with a drift rate of approximately 2.5 parts per billion (ppb). For comparison, an oven-controlled crystal oscillator (OCXO) has a drift rate of about 25 ppb, making the drift of the eNb effectively negligible.

For the eNb-to-SN link, the k -th SN receives the downlink frame with respect to (w.r.t.) its own clock at $T_{DL,k}$, which is formulated as

$$T_{DL,k} = t_n + \frac{d_{eNb,k}}{c} + \delta_{SN,k}, \quad (6)$$

where $\delta_{SN,k}$ represents the time offset of the k -th SN w.r.t. the eNb clock.

For the UE-to-SN link, the k -th SN receives the uplink frame w.r.t. its own clock at $T_{UL,k}$, which is expressed as

$$T_{UL,k} = T_{UE} + \frac{d_{UE,k}}{c} + \delta_{SN,k}, \quad (7)$$

Substituting T_{UE} from (5) into (7), we obtain

$$T_{UL,k} = t_n + \frac{d_{UB}}{c} - \delta_{TA} + \varepsilon_{UE} + \frac{d_{UE,k}}{c} + \delta_{SN,k}. \quad (8)$$

Since the UE's clock is synchronized to the eNb's clock, the reference to the UE's clock can be neglected in timing calculations.

C. Downlink & Uplink Subframe Timing Difference

Then, let us further model the downlink & uplink subframe timing difference, denoted as Δ_k , which can be measured by the open source code. Specifically, we have

$$\begin{aligned} \Delta_k &= T_{DL,k} - T_{UL,k} + \varepsilon_{SN,k} \\ &= \frac{d_{eNb,k}}{c} - \frac{d_{UB}}{c} - \frac{d_{UE,k}}{c} + \delta_{TA} - \varepsilon_{UE} + \varepsilon_{SN,k}, \end{aligned} \quad (9)$$

where $\varepsilon_{SN,k}$ denotes the measurement error at the k -th SN.

Reformulating (9), we have the following equation:

$$\frac{d_{UB}}{c} + \frac{d_{UE,k}}{c} = \frac{d_{eNb,k}}{c} + \Delta_k + \delta_{TA} - \varepsilon_{UE} + \varepsilon_{SN,k}, \quad (10)$$

This equation establishes a relationship between the distances involved and can be utilized to derive the estimated position of the UE.

III. LOCALIZATION SCHEME DESIGN

In this section, we design two kinds of localization scheme for estimating the unknown position of the UE.

A. ToA Based Localization Scheme

In this subsection, we present a ToA based localization scheme to estimate the unknown position of the UE. We utilize the timing difference measurements Δ_k from two SNs while ignoring hardware timing errors and measurement noise for simplicity [10].

Starting from (10), and neglecting the error terms ε_{UE} and $\varepsilon_{SN,k}$, we obtain

$$\frac{d_{UB}}{c} + \frac{d_{UE,k}}{c} \approx \frac{d_{eNb,k}}{c} + \Delta_k + \delta_{TA}, \quad (11)$$

where $k = 1, 2$ represents the index of the sniffers. Then, by multiplying both sides of (11) by c yields

$$d_{UB} + d_{UE,k} \approx d_{eNb,k} + c(\Delta_k + \delta_{TA}). \quad (12)$$

Let us further define $D_k = d_{eNb,k} + c(\Delta_k + \delta_{TA})$, we have

$$d_{UB} + d_{UE,k} \approx D_k. \quad (13)$$

Substituting the expressions for d_{UB} and $d_{UE,k}$ in terms of the positions, we have

$$\|\mathbf{u} - \mathbf{p}\| + \|\mathbf{u} - \mathbf{s}_k\| \approx D_k, \quad (14)$$

which represents that the sum of distances from the UE to the eNb and to the k -th sniffer equals a known constant D_k . This forms the basis of the ellipse intersection problem. Let us further assume two sniffers ($k = 1, 2$), we obtain two equations, which is given as [10]

$$\|\mathbf{u} - \mathbf{p}\| + \|\mathbf{u} - \mathbf{s}_1\| \approx D_1, \quad (15)$$

$$\|\mathbf{u} - \mathbf{p}\| + \|\mathbf{u} - \mathbf{s}_2\| \approx D_2. \quad (16)$$

These two ellipse equations can be used to estimate the UE's position $\mathbf{u} = [x_u, y_u]^T$ with direct numerical computation.

B. TDoA Based Localization Scheme

In the previous subsection, we directly ignored hardware timing errors and measurement noise to simplify the localization problem. However, in practical measurements, these errors cannot be neglected, as they significantly affect localization accuracy. To further reduce the impact of these errors, we consider using a TDoA based localization scheme.

Specifically, we first perform measurements with two SNs simultaneously. Then, keeping one SN fixed, we move the other to a different location. This approach allows us to collect measurements from different SN configurations while maintaining synchronization within the same time slot.

From (10), including the error terms, and considering the first measurement configuration with SNs at positions \mathbf{s}_1 and \mathbf{s}_2 , we have

$$\frac{d_{UB}}{c} + \frac{d_{UE,1}}{c} = \frac{d_{eNb,1}}{c} + \Delta_1 + \delta_{TA} - \varepsilon_{UE} + \varepsilon_{SN,1}, \quad (17)$$

$$\frac{d_{UB}}{c} + \frac{d_{UE,2}}{c} = \frac{d_{eNb,2}}{c} + \Delta_2 + \delta_{TA} - \varepsilon_{UE} + \varepsilon_{SN,2}. \quad (18)$$

By subtracting (18) from (17), we eliminate common terms such as d_{UB}/c , δ_{TA} , and ε_{UE} , resulting in a TDoA expression as

$$\begin{aligned} \Delta d_{12} &= d_{UE,1} - d_{UE,2} \\ &= d_{eNb,1} - d_{eNb,2} + c(\Delta_1 - \Delta_2) + c(\varepsilon_{SN,1} - \varepsilon_{SN,2}) \\ &= d_{eNb,12} + \delta_{1q} + \varepsilon_{1q}, \end{aligned} \quad (19)$$

where $d_{eNb,12} = d_{eNb,1} - d_{eNb,2}$, $\delta_{12} = c(\Delta_1' - \Delta_2)$, and $\varepsilon_{12} = c(\varepsilon_{SN,1} - \varepsilon_{SN,2})$.

Next, we move the 2-nd SN to a new location, at position \mathbf{s}_3 , while keeping the 1-st SN at \mathbf{s}_1 . We perform another set of measurements, and similar to (19), we obtain another TDoA expression as

$$\begin{aligned} \Delta d_{12} &= d_{UE,1} - d_{UE,3} \\ &= d_{eNb,1} - d_{eNb,3} + c(\Delta_1' - \Delta_3) + c(\varepsilon_{SN,1} - \varepsilon_{SN,3}) \\ &= d_{eNb,13} + \delta_{13} + \varepsilon_{13}, \end{aligned} \quad (20)$$

where $d_{eNb,13} = d_{eNb,1} - d_{eNb,3}$, $\delta_{13} = c(\Delta_1' - \Delta_3)$, and $\varepsilon_{13} = c(\varepsilon_{SN,1} - \varepsilon_{SN,3})$. Besides, Δ_1' and Δ_3 denote the measured time difference at \mathbf{s}_1 and \mathbf{s}_3 , respectively. Here, the errors ε_{12} and

ε_{13} are assumed to be small and can be modeled as random noise with zero mean.

Besides, we can express the distance differences Δd_{1k} $k \in \{2, 3\}$ in terms of the UE's position:

$$\begin{aligned} \Delta d_{1k} &= \sqrt{(x_k - x_u)^2 + (y_k - y_u)^2} \\ &\quad - \sqrt{(x_1 - x_u)^2 + (y_1 - y_u)^2} \\ \Rightarrow \Delta d_{1k} &+ \sqrt{(x_1 - x_u)^2 + (y_1 - y_u)^2} \\ &= \sqrt{(x_k - x_u)^2 + (y_k - y_u)^2}, \end{aligned} \quad (21)$$

Then, introducing $d_{UE,1} = \sqrt{(x_1 - x_u)^2 + (y_1 - y_u)^2}$ and squaring both sides of (21), we obtain the following set of hyperbola equation

$$\begin{aligned} (x_u - x_1)(x_k - x_1) + (y_u - y_1)(y_k - y_1) + \Delta d_{1k} \times d_{UE,1} \\ = \frac{1}{2} \left[(x_k - x_1)^2 + (y_k - y_1)^2 - \Delta d_{1k}^2 \right], \quad k = 2, 3 \end{aligned} \quad (22)$$

which represent hyperbolas on which the UE must lie. Writing (22) in matrix form gives

$$\mathbf{G}\boldsymbol{\vartheta} = \mathbf{h}, \quad (23)$$

where

$$\mathbf{G} = \begin{bmatrix} x_2 - x_1 & y_2 - y_1 & \Delta d_{12} \\ x_3 - x_1 & y_3 - y_1 & \Delta d_{13} \end{bmatrix}, \quad (24)$$

$$\mathbf{h} = \frac{1}{2} \begin{bmatrix} (x_2^2 + y_2^2) - (x_1^2 + y_1^2) - \Delta d_{12}^2 \\ (x_3^2 + y_3^2) - (x_1^2 + y_1^2) - \Delta d_{13}^2 \end{bmatrix}, \quad (25)$$

and the parameter $\boldsymbol{\vartheta} = [x_u, y_u, d_{UE,1}]^T$. Accordingly, we can formulate a LS problem [11] to estimate the UE's position \mathbf{u} .

1) *Formulating the LS Problem:* With the system in the form $\mathbf{G}\boldsymbol{\vartheta} = \mathbf{h}$, we can formulate the LS problem to estimate $\boldsymbol{\vartheta}$, which is given as

$$\min_{\boldsymbol{\vartheta}} J(\boldsymbol{\vartheta}) = \|\mathbf{G}\boldsymbol{\vartheta} - \mathbf{h}\|^2. \quad (26)$$

2) *Solving the LS Problem:* In the presence of measurement errors, we aim to find the parameter vector $\boldsymbol{\vartheta}$ that minimizes the cost function (26), which is a standard linear LS problem, which can be solved analytically. The optimal solution $\hat{\boldsymbol{\vartheta}}$ that minimizes $J(\boldsymbol{\vartheta})$ is obtained by solving the normal equations [11]:

$$\mathbf{G}^T \mathbf{G} \hat{\boldsymbol{\vartheta}} = \mathbf{G}^T \mathbf{h}. \quad (27)$$

Assuming $\mathbf{G}^T \mathbf{G}$ is invertible, the solution is given by

$$\hat{\boldsymbol{\vartheta}} = (\mathbf{G}^T \mathbf{G})^{-1} \mathbf{G}^T \mathbf{h}. \quad (28)$$

IV. EXPERIMENTAL RESULTS

Our experimental setup consists of two X310 software-defined radios (SDRs) running LTE Sniffer v2.1.0 and an iPhone SE serving as the UE. As shown in Fig. 1, the eNb is located at the S1 EEE building rooftop of NTU, operated by M1 service providers. The whole setup is located within TA = 1, where the internal boundary starts at 78.12 m and ends at 156.24 m, covering a total distance of 78.12 m. The UE, SN 1, and SN 2 are positioned on the S2 EEE rooftop at distances of 114.70 m, 109.70 m, and 139.50 m from the eNb, respectively. We positioned the UE in line of sight with

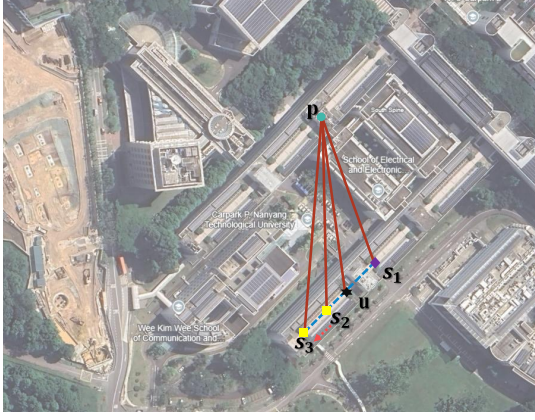


Fig. 1: Satellite image of two sniffers experiment setup.

the eNb to ensure optimal signal reception. For each distance measurement of the UE, we reconnected six times to measure the distance over multiple connections, enhancing the accuracy of our measurements.

From Fig. 1, we can observe that to achieve the TDoA effect, we fix SN 1 at position s_1 and move SN 2 from its initial position at s_2 (139.50 m from the eNb) to a new position at s_3 (154.0 m from the eNb).

Remark 1: Typically, implementing TDoA requires three sniffers; however, by moving one sniffer to another location and ensuring that during the same time period the two sniffers capture transmissions within the same subframe, we can achieve TDoA with only two sniffers.

Fig. 2 shows the terminal output of the sniffer's logging interface. The sniffer first tunes to the same Physical Cell ID (PCI) and eNb as the UE. The output consists of subframe identification numbers, followed by the RNTI of each detected user in the area. Once the target UE is identified, the recording switches to logging UE-specific data. As shown in Fig. 2, each log entry includes the downlink-uplink (DL-UL) timing difference in microseconds, corresponding to the subframe timing difference for the individual UE. The signal-to-noise ratio (SNR) and channel quality indicator (CQI) are also printed for each UE, along with noise power.

The average number of active users during data recording under the same eNb ranges from 80 to 190. To capture the target radio network temporary identifiers (RNTIs) among multiple RNTIs, we placed our UE in radio resource control (RRC) connection mode by toggling the network off and on to identify the target RNTI. Once identified, we initiated data recording for the UE. For extended data collection, we made a call to the UE to maintain the RNTI. Each dataset was recorded for 20 seconds, which is the minimum duration the UE retains the RNTI without an active call. In our experiment, UE position remained the same throughout the data recording. The plotted distance is calculated from the data points corresponding to the multiple delta values received during data collection.

We recorded data from SN 1 and SN 2 simultaneously to minimize the impact of random offset. To extract and match the delta value between the two sniffers, we first sorted the data

Time Frame number	Subframe Index number	RNTI	Timing difference
Frame 0	SP 115	RNTI: 52995	DL-UL (μs): 29.1
Frame 0	SP 116	RNTI: 52995	DL-UL (μs): 29.1
Frame 0	SP 117	RNTI: 52995	DL-UL (μs): 29.1
Frame 0	SP 118	RNTI: 52995	DL-UL (μs): 29.1
Frame 0	SP 119	RNTI: 52995	DL-UL (μs): 29.1
Frame 0	SP 120	RNTI: 52995	DL-UL (μs): 29.1
Frame 0	SP 121	RNTI: 52995	DL-UL (μs): 29.1
Frame 0	SP 122	RNTI: 52995	DL-UL (μs): 29.1
Frame 0	SP 123	RNTI: 52995	DL-UL (μs): 29.1
Frame 0	SP 124	RNTI: 52995	DL-UL (μs): 29.1
Frame 0	SP 125	RNTI: 52995	DL-UL (μs): 29.1
Frame 0	SP 126	RNTI: 52995	DL-UL (μs): 29.1
Frame 0	SP 127	RNTI: 52995	DL-UL (μs): 29.1
Frame 0	SP 128	RNTI: 52995	DL-UL (μs): 29.1
Frame 0	SP 129	RNTI: 52995	DL-UL (μs): 29.1
Frame 0	SP 130	RNTI: 52995	DL-UL (μs): 29.1
Frame 0	SP 131	RNTI: 52995	DL-UL (μs): 29.1
Frame 0	SP 132	RNTI: 52995	DL-UL (μs): 29.1
Frame 0	SP 133	RNTI: 52995	DL-UL (μs): 29.1
Frame 0	SP 134	RNTI: 52995	DL-UL (μs): 29.1
Frame 0	SP 135	RNTI: 52995	DL-UL (μs): 29.1
Frame 0	SP 136	RNTI: 52995	DL-UL (μs): 29.1
Frame 0	SP 137	RNTI: 52995	DL-UL (μs): 29.1
Frame 0	SP 138	RNTI: 52995	DL-UL (μs): 29.1
Frame 0	SP 139	RNTI: 52995	DL-UL (μs): 29.1
Frame 0	SP 140	RNTI: 52995	DL-UL (μs): 29.1
Frame 0	SP 141	RNTI: 52995	DL-UL (μs): 29.1
Frame 0	SP 142	RNTI: 52995	DL-UL (μs): 29.1
Frame 0	SP 143	RNTI: 52995	DL-UL (μs): 29.1
Frame 0	SP 144	RNTI: 52995	DL-UL (μs): 29.1
Frame 0	SP 145	RNTI: 52995	DL-UL (μs): 29.1
Frame 0	SP 146	RNTI: 52995	DL-UL (μs): 29.1
Frame 0	SP 147	RNTI: 52995	DL-UL (μs): 29.1
Frame 0	SP 148	RNTI: 52995	DL-UL (μs): 29.1
Frame 0	SP 149	RNTI: 52995	DL-UL (μs): 29.1
Frame 0	SP 150	RNTI: 52995	DL-UL (μs): 29.1
Frame 0	SP 151	RNTI: 52995	DL-UL (μs): 29.1
Frame 0	SP 152	RNTI: 52995	DL-UL (μs): 29.1
Frame 0	SP 153	RNTI: 52995	DL-UL (μs): 29.1
Frame 0	SP 154	RNTI: 52995	DL-UL (μs): 29.1
Frame 0	SP 155	RNTI: 52995	DL-UL (μs): 29.1
Frame 0	SP 156	RNTI: 52995	DL-UL (μs): 29.1
Frame 0	SP 157	RNTI: 52995	DL-UL (μs): 29.1
Frame 0	SP 158	RNTI: 52995	DL-UL (μs): 29.1
Frame 0	SP 159	RNTI: 52995	DL-UL (μs): 29.1
Frame 0	SP 160	RNTI: 52995	DL-UL (μs): 29.1
Frame 0	SP 161	RNTI: 52995	DL-UL (μs): 29.1
Frame 0	SP 162	RNTI: 52995	DL-UL (μs): 29.1
Frame 0	SP 163	RNTI: 52995	DL-UL (μs): 29.1
Frame 0	SP 164	RNTI: 52995	DL-UL (μs): 29.1
Frame 0	SP 165	RNTI: 52995	DL-UL (μs): 29.1
Frame 0	SP 166	RNTI: 52995	DL-UL (μs): 29.1
Frame 0	SP 167	RNTI: 52995	DL-UL (μs): 29.1
Frame 0	SP 168	RNTI: 52995	DL-UL (μs): 29.1
Frame 0	SP 169	RNTI: 52995	DL-UL (μs): 29.1
Frame 0	SP 170	RNTI: 52995	DL-UL (μs): 29.1
Frame 0	SP 171	RNTI: 52995	DL-UL (μs): 29.1
Frame 0	SP 172	RNTI: 52995	DL-UL (μs): 29.1
Frame 0	SP 173	RNTI: 52995	DL-UL (μs): 29.1
Frame 0	SP 174	RNTI: 52995	DL-UL (μs): 29.1
Frame 0	SP 175	RNTI: 52995	DL-UL (μs): 29.1
Frame 0	SP 176	RNTI: 52995	DL-UL (μs): 29.1
Frame 0	SP 177	RNTI: 52995	DL-UL (μs): 29.1
Frame 0	SP 178	RNTI: 52995	DL-UL (μs): 29.1
Frame 0	SP 179	RNTI: 52995	DL-UL (μs): 29.1
Frame 0	SP 180	RNTI: 52995	DL-UL (μs): 29.1
Frame 0	SP 181	RNTI: 52995	DL-UL (μs): 29.1
Frame 0	SP 182	RNTI: 52995	DL-UL (μs): 29.1
Frame 0	SP 183	RNTI: 52995	DL-UL (μs): 29.1
Frame 0	SP 184	RNTI: 52995	DL-UL (μs): 29.1
Frame 0	SP 185	RNTI: 52995	DL-UL (μs): 29.1
Frame 0	SP 186	RNTI: 52995	DL-UL (μs): 29.1
Frame 0	SP 187	RNTI: 52995	DL-UL (μs): 29.1
Frame 0	SP 188	RNTI: 52995	DL-UL (μs): 29.1
Frame 0	SP 189	RNTI: 52995	DL-UL (μs): 29.1
Frame 0	SP 190	RNTI: 52995	DL-UL (μs): 29.1
Frame 0	SP 191	RNTI: 52995	DL-UL (μs): 29.1
Frame 0	SP 192	RNTI: 52995	DL-UL (μs): 29.1
Frame 0	SP 193	RNTI: 52995	DL-UL (μs): 29.1
Frame 0	SP 194	RNTI: 52995	DL-UL (μs): 29.1
Frame 0	SP 195	RNTI: 52995	DL-UL (μs): 29.1
Frame 0	SP 196	RNTI: 52995	DL-UL (μs): 29.1
Frame 0	SP 197	RNTI: 52995	DL-UL (μs): 29.1
Frame 0	SP 198	RNTI: 52995	DL-UL (μs): 29.1
Frame 0	SP 199	RNTI: 52995	DL-UL (μs): 29.1
Frame 0	SP 200	RNTI: 52995	DL-UL (μs): 29.1
Frame 0	SP 201	RNTI: 52995	DL-UL (μs): 29.1
Frame 0	SP 202	RNTI: 52995	DL-UL (μs): 29.1
Frame 0	SP 203	RNTI: 52995	DL-UL (μs): 29.1
Frame 0	SP 204	RNTI: 52995	DL-UL (μs): 29.1
Frame 0	SP 205	RNTI: 52995	DL-UL (μs): 29.1
Frame 0	SP 206	RNTI: 52995	DL-UL (μs): 29.1
Frame 0	SP 207	RNTI: 52995	DL-UL (μs): 29.1
Frame 0	SP 208	RNTI: 52995	DL-UL (μs): 29.1
Frame 0	SP 209	RNTI: 52995	DL-UL (μs): 29.1
Frame 0	SP 210	RNTI: 52995	DL-UL (μs): 29.1
Frame 0	SP 211	RNTI: 52995	DL-UL (μs): 29.1
Frame 0	SP 212	RNTI: 52995	DL-UL (μs): 29.1
Frame 0	SP 213	RNTI: 52995	DL-UL (μs): 29.1
Frame 0	SP 214	RNTI: 52995	DL-UL (μs): 29.1
Frame 0	SP 215	RNTI: 52995	DL-UL (μs): 29.1
Frame 0	SP 216	RNTI: 52995	DL-UL (μs): 29.1
Frame 0	SP 217	RNTI: 52995	DL-UL (μs): 29.1
Frame 0	SP 218	RNTI: 52995	DL-UL (μs): 29.1
Frame 0	SP 219	RNTI: 52995	DL-UL (μs): 29.1
Frame 0	SP 220	RNTI: 52995	DL-UL (μs): 29.1
Frame 0	SP 221	RNTI: 52995	DL-UL (μs): 29.1
Frame 0	SP 222	RNTI: 52995	DL-UL (μs): 29.1
Frame 0	SP 223	RNTI: 52995	DL-UL (μs): 29.1
Frame 0	SP 224	RNTI: 52995	DL-UL (μs): 29.1
Frame 0	SP 225	RNTI: 52995	DL-UL (μs): 29.1
Frame 0	SP 226	RNTI: 52995	DL-UL (μs): 29.1
Frame 0	SP 227	RNTI: 52995	DL-UL (μs): 29.1
Frame 0	SP 228	RNTI: 52995	DL-UL (μs): 29.1
Frame 0	SP 229	RNTI: 52995	DL-UL (μs): 29.1
Frame 0	SP 230	RNTI: 52995	DL-UL (μs): 29.1
Frame 0	SP 231	RNTI: 52995	DL-UL (μs): 29.1
Frame 0	SP 232	RNTI: 52995	DL-UL (μs): 29.1
Frame 0	SP 233	RNTI: 52995	DL-UL (μs): 29.1
Frame 0	SP 234	RNTI: 52995	DL-UL (μs): 29.1
Frame 0	SP 235	RNTI: 52995	DL-UL (μs): 29.1
Frame 0	SP 236	RNTI: 52995	DL-UL (μs): 29.1
Frame 0	SP 237	RNTI: 52995	DL-UL (μs): 29.1
Frame 0	SP 238	RNTI: 52995	DL-UL (μs): 29.1
Frame 0	SP 239	RNTI: 52995	DL-UL (μs): 29.1
Frame 0	SP 240	RNTI: 52995	DL-UL (μs): 29.1
Frame 0	SP 241	RNTI: 52995	DL-UL (μs): 29.1
Frame 0	SP 242	RNTI: 52995	DL-UL (μs): 29.1
Frame 0	SP 243	RNTI: 52995	DL-UL (μs): 29.1
Frame 0	SP 244	RNTI: 52995	DL-UL (μs): 29.1
Frame 0	SP 245	RNTI: 52995	DL-UL (μs): 29.1
Frame 0	SP 246	RNTI: 52995	DL-UL (μs): 29.1
Frame 0	SP 247	RNTI: 52995	DL-UL (μs): 29.1
Frame 0	SP 248	RNTI: 52995	DL-UL (μs): 29.1
Frame 0	SP 249	RNTI: 52995	DL-UL (μs): 29.1
Frame 0	SP 250	RNTI: 52995	DL-UL (μs): 29.1
Frame 0	SP 251	RNTI: 52995	DL-UL (μs): 29.1
Frame 0	SP 252	RNTI: 52995	DL-UL (μs): 29.1
Frame 0	SP 253	RNTI: 52995	DL-UL (μs): 29.1
Frame 0	SP 254	RNTI: 52995	DL-UL (μs): 29.1
Frame 0	SP 255	RNTI: 52995	DL-UL (μs): 29.1
Frame 0	SP 256	RNTI: 52995	DL-UL (μs): 29.1
Frame 0	SP 257	RNTI: 52995	DL-UL (μs): 29.1
Frame 0	SP 258	RNTI: 52995	DL-UL (μs): 29.1
Frame 0	SP 259	RNTI: 52995	DL-UL (μs): 29.1
Frame 0	SP 260	RNTI: 52995	DL-UL (μs): 29.1
Frame 0	SP 261	RNTI: 52995	DL-UL (μs): 29.1
Frame 0	SP 262	RNTI: 52995	DL-UL (μs): 29.1
Frame 0	SP 263	RNTI: 52995	DL-UL (μs): 29.1
Frame 0	SP 264	RNTI: 52995	DL-UL (μs): 29.1
Frame 0	SP 265	RNTI: 52995	DL-UL (μs): 29.1
Frame 0	SP 266	RNTI: 52995	DL-UL (μs): 29.1
Frame 0	SP 267	RNTI: 52995	DL-UL (μs): 29.1
Frame 0	SP 268	RNTI: 52995	DL-UL (μs): 29.1
Frame 0	SP 269	RNTI: 52995	DL-UL (μs): 29.1
Frame 0	SP 270	RNTI: 52995	DL-UL (μs): 29.1
Frame 0	SP 271	RNTI: 52995	DL-UL (μs): 29.1
Frame 0	SP 272	RNTI: 52995	DL-UL (μs): 29.1
Frame 0	SP 273	RNTI: 52995	DL-UL (μs): 29.1
Frame 0	SP 274	RNTI: 52995	DL-UL (μs): 29.1
Frame 0	SP 275	RNTI: 52995	DL-UL (μs): 29.1
Frame 0	SP 276	RNTI: 52995	DL-UL (μs): 29.1
Frame 0	SP 277	RNTI: 52995	DL-UL (μs): 29.1
Frame 0	SP 278	RNTI: 52995	DL-UL (μs): 29.1
Frame 0	SP 279	RNTI: 52995	DL-UL (μs): 29.1
Frame 0	SP 280	RNTI: 52995	DL-UL (μs): 29.1
Frame 0	SP 281	RNTI: 52995	DL-UL (μs): 29.1
Frame 0	SP 282	RNTI: 52995	DL-UL (μs): 29.1
Frame 0	SP 283	RNTI: 52995	DL-UL (μs): 29.1
Frame 0	SP 284	RNTI: 52995	DL-UL (μs): 29.1
Frame 0	SP 285	RNTI: 52995	DL-UL (μs): 29.1
Frame 0	SP 286	RNTI: 52995	DL-UL (μs): 29.1
Frame 0	SP 287	RNTI: 52995	DL-UL (μs): 29.1
Frame 0	SP 288	RNTI: 52995	DL-UL (μs): 29.1
Frame 0	SP 289	RNTI: 52995	DL-UL (μs): 29.1
Frame 0	SP 290	RNTI: 52995	DL-UL (μs): 29.1
Frame 0	SP 291	RNTI: 52995	DL-UL (μs): 29.1
Frame 0	SP 292	RNTI: 52995	DL-UL (μs): 29.1
Frame 0	SP 293	RNTI: 52995	DL-UL (μs): 29.1
Frame 0	SP 294	RNTI: 52995	DL-UL (μs): 29.1
Frame 0	SP 295	RNTI: 52995	DL-UL (μs): 29.1
Frame 0	SP 296	RNTI: 52995	DL-UL (μs): 29.1
Frame 0	SP 297	RNTI: 52995	DL-UL (μs): 29.1
Frame 0	SP 298	RNTI: 52995	DL-UL (μs): 29.1
Frame 0	SP 299	RNTI: 52995	DL-UL (μs): 29.1
Frame 0	SP 300	RNTI: 52995	DL-UL (μs): 29.1
Frame 0	SP 301	RNTI: 52995	DL-UL (μs): 29.1
Frame 0	SP 302	RNTI: 52995	DL-UL (μs): 29.1
Frame 0	SP 303	RNTI: 52995	DL-UL (μs): 29.1
Frame 0	SP 304	RNTI: 52995	DL-UL (μs): 29.1
Frame 0	SP 305	RNTI: 52995	DL-UL (μs): 29.1
Frame 0	SP 306	RNTI: 52995	DL-UL (μs): 29.1
Frame 0	SP 307	RNTI: 52995	DL-UL (μs): 29.1
Frame 0	SP 308	RNTI: 52995	DL-UL (μs): 29.1
Frame 0	SP 309	RNTI: 52995	DL-UL (μs): 29.1
Frame 0	SP 310	RNTI: 52995	DL-UL (μs): 29.1
Frame 0	SP 311	RNTI: 52995	DL-UL (μs): 29.1
Frame 0	SP 312	RNTI: 52995	DL-UL (μs): 29.1
Frame 0	SP 313	RNTI: 52995	DL-UL (μs): 29.1
Frame 0	SP 314	RNTI: 52995	DL-UL (μs): 29.1
Frame 0	SP 315	RNTI: 52995	DL-UL (μs): 29.1
Frame 0	SP 316	RNTI: 52995	DL-UL (μs): 29.1
Frame 0	SP 317	RNTI: 52995	DL-UL (μs): 29.1
Frame 0	SP 318	RNTI: 52995	DL-UL (μs): 29.1
Frame 0	SP 319	RNTI: 52995	DL-UL (μs): 29.1
Frame 0	SP 320	RNTI: 52995	DL-UL (μs): 29.1</

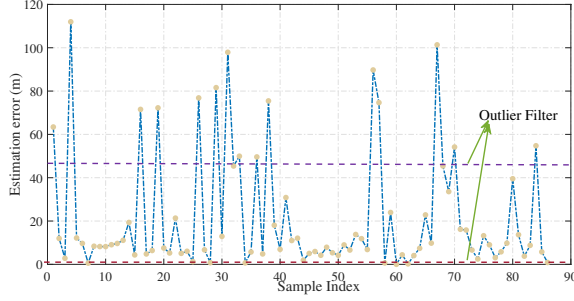


Fig. 4: TDoA measurement in 20dB.

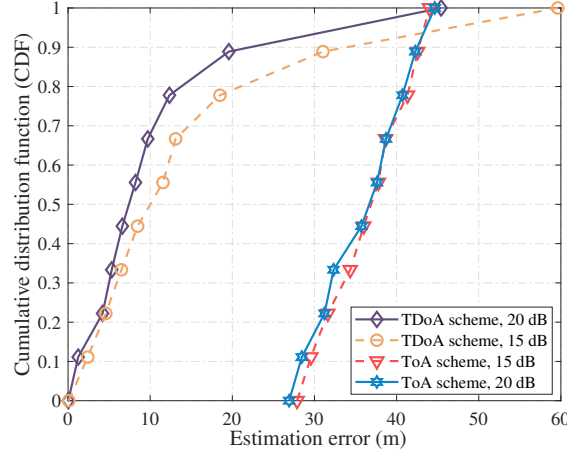


Fig. 5: CDF of ToA and TDoA schemes at 15 dB and 20 dB.

the mean distance error before filtering was 21.44 m, which was further reduced to 10.12 m after filtering. This improved accuracy highlights the scheme's effectiveness, especially for applications in security-sensitive fields where precise localization is critical.

Fig. 5 presents the cumulative distribution function (CDF) of the ToA and TDoA schemes under signal conditions of 15 dB and 20 dB. From Fig. 5, it is evident that increasing the SNR has little effect on improving the localization accuracy when using the ToA scheme, the results remain nearly unchanged regardless of the increase in SNR. In contrast, the TDoA scheme shows a significant improvement in accuracy as the SNR increases. Specifically, the estimation errors at the 80% probability level are approximately 11 m and 20 m for 20 dB and 15 dB, respectively, when using the TDoA scheme.

The observation from Fig. 5 highlights the fact that the TDoA scheme benefits greatly from higher SNR, resulting in more accurate localization. *Therefore, to achieve optimal localization accuracy, it is preferable to operate under high SNR conditions when applying the TDoA scheme.* However, in practical applications, it is also important to consider the trade-off between localization accuracy and detection cost. Higher accuracy generally requires the detection of more subframes, which may increase the overall computational and energy cost of the system. *In most security-related applications, a signal condition of 15 dB is sufficient to meet localization accuracy requirements, offering a reasonable balance between performance and operational efficiency without significantly*

increasing resource usage. Thus, while higher SNR is ideal, the 15 dB condition provides an acceptable compromise for most practical uses.

Scheme	Mean	RMSE	STD
ToA	36.83 m	36.52 m	4.79 m
TDoA	13.99 m	10.12 m	9.65 m

TABLE I: Comparison for ToA and TDoA schemes.

Table I provides a comparison of the mean, root mean square error (RMSE), and standard deviation (STD) for the ToA and TDoA schemes. It is evident that the TDoA scheme outperforms the ToA scheme in terms of localization accuracy. Specifically, the Mean and RMSE for TDoA are significantly lower, at 13.99 m and 10.12 meters, respectively, compared to 36.83 m and 36.52 m for ToA. This demonstrates a notable improvement in estimation precision when employing the TDoA approach. Furthermore, the TDoA scheme exhibits a larger standard deviation (9.65 m) compared to ToA (4.79 m), indicating greater variability in the distance errors, which can be attributed to the additional measurements and processing required for the TDoA calculations. Overall, the TDoA scheme achieves better accuracy and lower RMSE, making it more suitable for applications that demand precise localization.

V. CONCLUSION

We investigated a dual-sniffer passive localization system for locating UE in densely populated urban environments. Two localization schemes were developed: a ToA based scheme and a TDoA based scheme. Simulation results validated the effectiveness of the proposed TDoA-based scheme, demonstrating improved accuracy in UE positioning.

REFERENCES

- [1] S. Lu *et al.*, "Integrated sensing and communications: Recent advances and ten open challenges," *IEEE Internet Things J.*, vol. 11, no. 11, pp. 19 094–19 120, 2024.
- [2] H. Niu *et al.*, "Artificial noise elimination without the transmitter–receiver link csi," *IEEE Trans. Veh. Technol.*, vol. 73, no. 9, pp. 13 206–13 218, 2024.
- [3] A. Yassin *et al.*, "Recent advances in indoor localization: A survey on theoretical approaches and applications," *IEEE Commun. Surv. Tutor.*, vol. 19, no. 2, pp. 1327–1346, 2017.
- [4] Y. Tian, Y. He, and H. Duan, "Passive localization through channel estimation of on-the-air lte signals," *IEEE Access*, vol. 7, pp. 160 029–160 042, 2019.
- [5] L. Karaçay *et al.*, "A network-based positioning method to locate false base stations," *IEEE Access*, vol. 9, pp. 111 368–111 382, 2021.
- [6] R. Falkenberg and C. Wietfeld, "Falcon: An accurate real-time monitor for client-based mobile network data analytics," in *2019 IEEE Global Communications Conference (GLOBECOM)*. IEEE, 2019, pp. 1–7.
- [7] T. Wu *et al.*, "Joint angle estimation error analysis and 3-d positioning algorithm design for mmwave positioning system," *IEEE Internet Things J.*, vol. 11, no. 2, pp. 2181–2197, 2024.
- [8] M. Kotuliak *et al.*, "LTrack: Stealthy tracking of mobile phones in LTE," in *31st USENIX Security Symposium (USENIX Security 22)*, 2022, pp. 1291–1306.
- [9] T. Wu *et al.*, "Exploit high-dimensional ris information to localization: What is the impact of faulty element?" *IEEE J. Sel. Areas Commun.*, vol. 42, no. 10, pp. 2803–2819, 2024.
- [10] J. Smith and J. Abel, "Closed-form least-squares source location estimation from range-difference measurements," *IEEE Trans. Acoust., Speech, Signal Process.*, vol. 35, no. 12, pp. 1661–1669, 1987.
- [11] Y. Chan and K. Ho, "A simple and efficient estimator for hyperbolic location," *IEEE Trans. Signal Process.*, vol. 42, no. 8, pp. 1905–1915, 1994.